Development of a Monte Carlo Simulator for the *Astro-E2* Hard X-Ray Detector (HXD-II)

Yukikatsu Terada, Shin Watanabe, Masanori Ohno, Masaya Suzuki, Takeshi Itoh, Isao Takahashi, Goro Sato, Mio Murashima, Naomi Kawano, Yasunobu Uchiyama, Shin Kubo, Tadayuki Takahashi, Makoto Tashiro, Motohide Kokubun, Kazuo Makishima, Tsuneyoshi Kamae, Toshio Murakami, Masaharu Nomachi, Yasushi Fukazawa, Kazutaka Yamaoka, Kazuhiro Nakazawa, and Daisuke Yonetoku

***Abstract*—The Hard X-ray Detector (HXD-II) is one of the scientific payloads on board the fifth Japanese cosmic X-ray satellite *Astro-E2*, scheduled for launch in 2005. The HXD-II is designed to cover a wide energy range of 10–600 keV with a high sensitivity of about 10^{-5} cnt/s/cm^2/keV. In order to derive the energy response of the sensor and to estimate the background, a Monte Carlo simulator based on the Geant4 toolkit is currently being developed. This paper describes the design concept of the HXD-II software package, including the analysis tools and the Monte Carlo simulator, and its verification through a comparison with actual data taken by pre-flight radio-isotope irradiation experiments, together with calculated outputs that can demonstrate the in-orbit performance of the HXD-II.**

***Index Terms*—Astronomical satellites, gamma-ray spectroscopy detectors, Monte Carlo, simulation.**

I. Introduction
Astro-E2 Hard X-Ray Detector (HXD-II)

IT IS difficult to conduct high-sensitivity spectroscopy in the hard X-ray to soft gamma-ray energy bandpass. The detector response is complicated, because the Compton-scattering process becomes dominant rather than photoelectric absorption; also, due to the Compton-scattering process, the arrival direction and the energy of the incident photons are lost. Furthermore, the source intensity of astrophysical objects at that energy range is usually weaker than the detector background, so that the sensitivity is mainly limited by the background level. In orbit, background events arise due to diffuse gamma-ray emission, non X-ray events caused directly by primary and secondary cosmic-rays, and sometimes by solar particle events; also important are radio-activated nuclei inside the detector induced by MeV protons trapped in the South Atlantic Anomaly (SAA). Therefore, to study the energy response and to estimate the time-variable background level become important issues, since they directly affect to the performance of the detector.

The Hard X-ray Detector (HXD) on-board *Astro-E*, the fifth Japanese astrophysical satellite, was devoted to the study of high-energy phenomena in the universe in the X-ray to soft gamma-ray region of 0.5–600 keV. It was designed and developed for over ten years, particularly to archive a sufficiently low background level [1]–[4]. The HXD covers a higher energy region of the mission, 10–600 keV, with a high sensitivity of about 10^{-5} cnt/s/cm^2/keV [5], [6]. Although the launch of *Astro-E* was unsuccessful in February, 2000, a recovery mission, *Astro-E2* was successfully launched on July 10, 2005, named Suzaki. The mission concept is essentially the same as *Astro-E*. In redesigning and developing the recovery instrument for the lost HXD, called HXD-II, a limited number of improvements ware introduced, as reported by Kokubun *et al.* [6].

As shown in Fig. 1, the HXD-II sensor consists of 16 identical GSO/BGO well-type-phoswich counters [7] incorporating 2 mm-thick silicon PIN diodes [8] (called Well Units), and surrounding 20 BGO shield counters (each called Anti Unit). In addition to the advantage of dramatically reducing the dead time in the electronics, this compound-eye configuration enables us

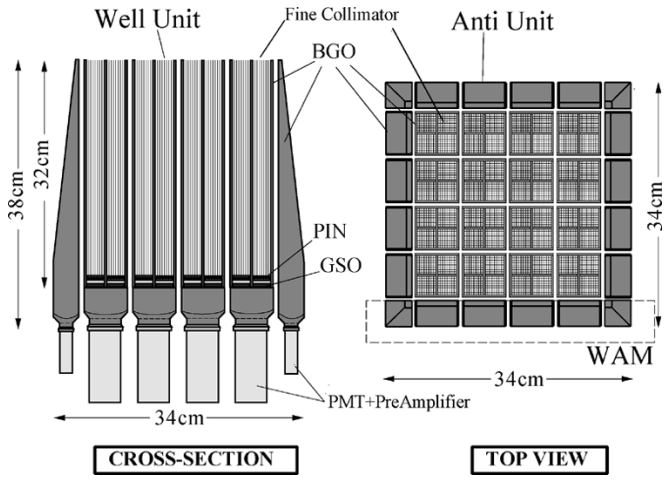

Fig. 1. Schematic view of the HXD-II sensor.

Manuscript received November 14, 2004; revised April 14, 2005.

Y. Terada is with the Institute of Physical and Chemical Research (RIKEN), Wako, Saitama 351-0198, Japan (e-mail: terada@riken.jp).

S. Watanabe, G. Sato, Y. Uchiyama, S. Kubo, T. Takahashi, and K. Nakazawa are with Institute of Space and Astronautical Science, Japan Aerospace Exploration Agency (ISAS/JAXA), Kanagawa 229-8510, Japan.

M. Ohno, N. Kawano, and Y. Fukazawa are with Department of Physics, Science, Hiroshima University, Hiroshima 739-8526, Japan.

M. Suzuki and M. Tashiro are with Department of Physics, Science, Saitama University, Saitama 338-8570, Japan.

T. Itoh, I. Takahashi, M. Murashima, and M. Kokubun are with Department of Physics, Science, University of Tokyo, Tokyo 113-0033, Japan.

K. Makisima is with RIKEN and the University of Tokyo, Tokyo 113-0033, Japan.

T. Kamae is with Stanford Linear Accelerator Center (SLAC), Menlo Park, CA 94025 USA.

T. Murakami and D. Yonetoku are with Department of Physics, Science, Kanazawa University, Kanazawa 920-1192, Japan.

M. Nomachi is with Department of Physics, Science, Osaka University, Osaka 560-0043, Japan.

K. Yamaoka is with Department of Physics and Mathematics, Aoyama Gakuin University, Kanagawa 229-8558, Japan.

Digital Object Identifier 10.1109/TNS.2005.852681

0018-9499/$20.00 © 2005 IEEE

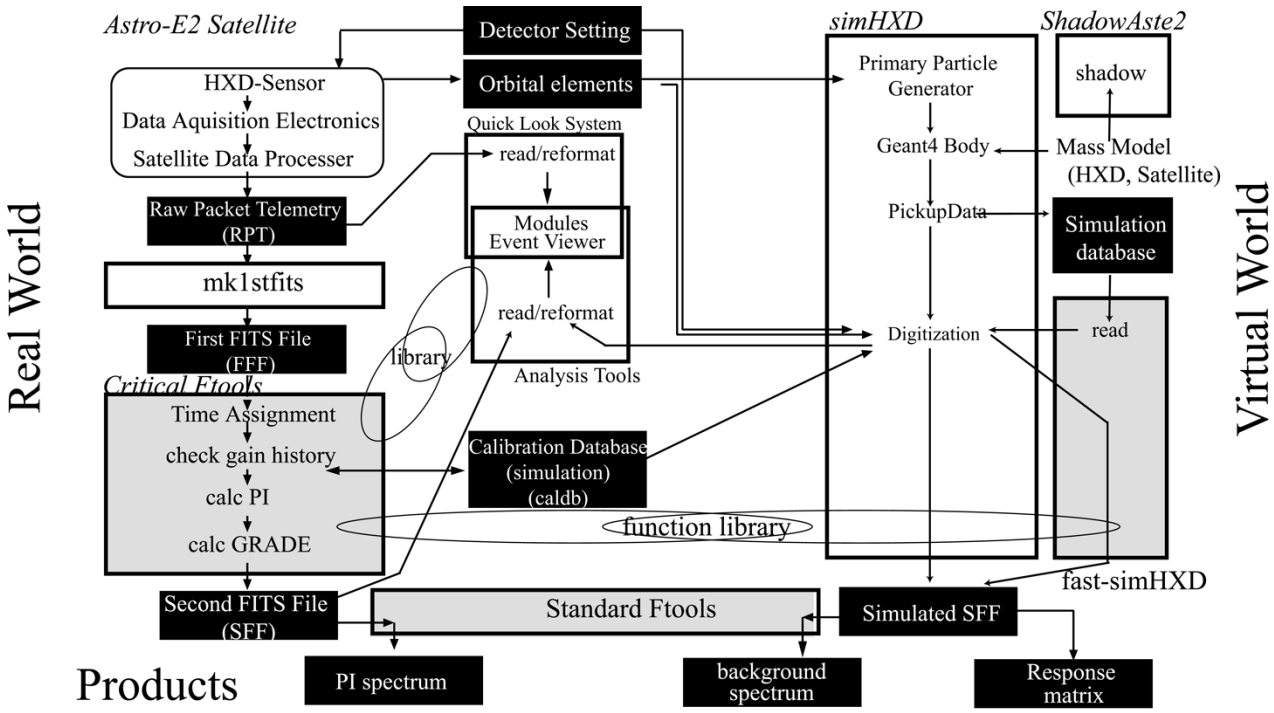

Fig. 2. Summary of the HXD-II software. Data files are shown in filled black boxes, and software tools are in box frames. The shaded and open boxes mean the public and private (accessible only for hardware team) tools, respectively.

to remove residual non X-ray backgrounds through anti-coincidence rejection in off-line analyses. This rejection is utilized by hit information from the 36 units, named HIT_PATTERN.

Main photo-absorbing materials of Well Units are GSO crystals and PIN diodes, which are installed at the bottom inside of a well-shaped BGO shield crystal with a narrow ($4^\circ \times 4^\circ$) opening. The GSO crystals are in optical and mechanical contact with the BGO shield part, and the output signal is read out by a single PMT per Well unit. Charged particles, nonaperture photons, and Compton-scattered events are efficiently rejected by on-board electronics [9] and off-line analysis, with a pulse shape discrimination (PSD) technique which utilizes the difference in the scintillation-decay-time constants between GSO (about 120 ns at -20 °C) and BGO (about 700 ns) crystals [2]. The PSD system of the HXD-II employs double-integration method; i.e., the pre-amplifier output is split into two shaping chains with different time constants, 150 ns (fast shaping) and 1000 ns (slow shaping), and the events hitting BGOs can be tagged by comparing the fast and slow shaping pulse heights.

In addition to on-axis observations of astrophysical objects, the HXD can achieve an all-sky monitoring observation, called HXD-Wideband All-sky Monitor (WAM), utilizing the 20 Anti Units, as described by Yamaoka *et al.* [10].

II. Development of the HXD-II Software Packages

A. Overview of the HXD-II Software

The final goal of the HXD-II observation is, needless to say, to obtain incident energy spectra including its normalization and time variation if any of astrophysical objects. For that purpose, the study of systematic errors both in the detector response and in the estimated background spectrum is an important subject. The final goal is to prepare the energy responses of the HXD-II with 5% accuracy and reproduce the background within 10% systematics.

The response matrix must be prepared for several event-selection modes with continuous energy bins, whereas only a few limited response for limited energies are available from radioactive isotope (RI) irradiation tests. Thus, a Monte Carlo simulator, which can calculate for photons with arbitrary energies, must be very useful. As for the background estimation, the difficulty in the spacecraft experiment lies in the fact that the input is a mixture of many types of non X-ray backgrounds, which in different and sometimes unpredictable ways. Therefore, we need a full Monte Carlo simulator including hadronic physics in MeV energies with activation processes, in addition to the electromagnetic process for photons.

The simulation toolkit is developed as one package of the HXD-II software utility. It includes a quick-look real-time system, data-processing tools, off-line analysis tools, and a calibration database, as summarized in Fig. 2. Among them, there are private tools locally used only by our hardware team; some private tools are optimized to process raw data, called Row Packet Telemetry (RPT) file, which is a direct dump of the satellite telemetry. After launch, nobody is allowed to access RPTs, because of our strong policy of the software: 1) to avoid the presence of multiple paths the data; 2) to wake all information available to end users. Thus, some private tools will be frozen and closed (or strictly limited in its use) after launch. At the same time, the algorithms in private tools have been very well tested. To compromise these requirements, core functions are gathered into libraries and shared between the private and public tools.

All HXD tools are operated on a framework named ANL, which was developed from the 1990s for the *ASCA* satellite, the preceding X-ray mission to *Astro-E*. The ANL is designed on the basic concept that a complicated process can be decomposed into many simple modules, and can be described as a chain of them [11]. An ANL module includes an initial function, a function for event-by-event analysis, and a termination function. The ANL framework calls these modules in the order defined by the chain. The actually implemented HXD-II tools are based on ASTE_ANL and/or anlplus framework, which are written in C and C++ languages, respectively, whereas the original ANL code is in FORTRAN.

B. Pulse-Height Invariant Space

To measure a source energy spectrum, a direct inverse transformation of the response matrix from the measured pulse heights (PHs) into the incident photon energies (IEs) is subject to large uncertainties, because the response matrix generally has many nondiagonal terms (i.e., the incident information is degenerated in the PH space). Therefore, the derivation of a source energy spectrum is not performed in the IE space, but in a modified PH space, called the pulse height invariant (PI), as detailed later. In deriving the source IE spectrum, analyzers first select an emission model, restricting its many free parameters into a small number. Then, they generate many trial PI distributions using the detector response, compare them with the background-subtracted actual PI data by a fitting method, and finally arrive at the best fit model. Thus, the background spectra and the response matrix must be prepared in the PI space.

Among characteristics, some are taken into account the process of the PH to PI conversion, while the others by the response matrix. The former includes:

- time-dependent gain trend of individual PMTs and PINs;
- nonlinearity of light yield (LY) of each GSO crystal as a function of the incident energy [7];
- nonlinearity of the electronics, including charge sensitive amplifiers, gain amplifiers, and the analog-to-digital converter (ADC);
- differential non linearities of the ADC;
- dead-time correction in the exposure time.

The characteristics included in a response matrix are:

- sensor geometries; in addition to shapes and lengths, degree of miss-alignments of the Well units and fine collimators, the effective area of the PIN diodes [8], and so on;
- material attributes, included several of our measurements of the photo-absorption coefficient;
- LYs of the BGO and GSO crystals of 20 individual units, including the light collection efficiency; LY for each component, such as BGO well part, BGO bottom part, and GSO, for Well units, and position dependence for Anti units [12];
- energy resolution of the PMTs and the PIN detectors;
- charge-correction efficiencies of the PIN diode [8];
- spreadings in the PSD circuit of each channel.

The event-selection criteria must be the same in the actually observed PI data and the response. Utilizing the trigger condition, quality flags, HIT_PATTERN and ADC values in the telemetry data [9], each event is tagged with a set of additional flags called GRADEs, which are defined as follows:

- GRADE_QUALTY (if the value is 1, some hardware trouble occurred, 0 others);
- GRADE_PMTTRG (if 0, the event is trigged only by a PMT anode channel);
- GRADE_PINTRG (if 0, the event is trigged only by a single PIN channel);
- GRADE_PSDSEL (GSO likelihood level in slow and fast pulse shaping PHA/PI space);
- GRADE_HITPAT (if the value is 0 or 1, there is no hit in the 8 or 4 surrounding units, respectively).

For example, pure PMT events can be extracted from the observational data, with a criterion of (GRADE_QUALTY $==0$ and GRADE_PMTTRG $==0$ and GRADE_PSDEL $<=3.0$ and GRADE_HITPAT $==1$); Similarly, pure PIN events with (GRADE_QUALTY $==0$ and GRADE_PINTRG $==0$ and GRADE_HITPAT $==1$). The same algorithm to determine these GRADEs are also employed in the HXD simulator to be described later (Section II-D).

C. Processing Tools for Actual Data

As summarized in Fig. 2, two sets of public data in FITS format (or Flexible Image Transport System; an astronomical standard format, endorsed by NASA and IAU) are prepared for each observation; First FITS File (FFF), which is just converted from RPT with no additional information, and Second FITS File (SFF), which have the same format as FFF, but with some processed information such as PI and GRADEs. FFFs are converted to SFFs using public-domain software called *critical ftools*. Among them, those dealing with the HXD-II data are developed by the HXD-II team, and released via the NASA GSFC software collaboration group as the HEADAS package. The products, such as the energy spectrum in PI space, are obtained by the public-domain standard *ftools* with the public-domain calibration data base, caldb.

The *critical ftools* for the HXD-II are separated into four tasks, and are used in the process in the following order. First, an FFF is processed by a time-assignment task, called *hxdtime*, which calculates arrival times of individual events, using each latched value of timing counters in the electronics, the satellite time at which the event was edited into a telemetry packet, and time stamps at the down-link timing to the ground station. Second, *mkhxdgainhist* task follows long-term gain histories of the individual PMTs utilizing intrinsic ^{152}Gd background peak, and creates a history table, which is included into the calibration database. Finally, the PI and GRADE calculation processes, called *hxdpi* and *hxdgrade*, respectively, are performed, according to the specifications already described (Section II-B).

D. Monte Carlo Simulator for the HXD-II

An HXD-II Monte Carlo simulator has been developed, called *simHXD*, based on the Geant4 toolkit [13] working on the anlplus framework (Section II-A) As shown in Fig. 2, the *simHXD* is separated into mainly four ANL modules: 1) the primary event generation part, 2) the geometry construction

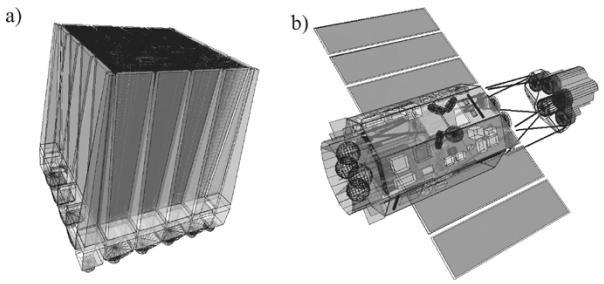

Fig. 3. (a) Constructed geometry models of the HXD-II sensor employed *simHXD*. (b) That of the *Astro-E2* satellite.

part with the Geant4 body driving the selected physics engine, 3) the module to pickup the hit information, and 4) the digitization part. A simple event-generation module (creating monochromatic photons) can be switched into a Cosmic-ray generation module, which irradiates particles with empirical energy spectra, while referring to orbital elements, solar activities, and so on. The geometry is selectable between the HXD-II sensor geometry and that of the entire spacecraft, as shown in Fig. 3(a) and (b), respectively.

The Geant4 engine generates hit information, such as energies deposited to the material, hit positions, and the particle type that causes the process; they are gathered and collected by the PickUpData module. Then, the digitization module calculates the output charge of the sensor devices, and converts them into digitalized values, while considering the response of the sensor and the properties of the electronics. The outputs have the same data format as that of the other tools, like the *critical ftools*, off-line analysis tools and quick look systems. Therefore, many ANL modules in the *critical ftools* can be installed into *simHXD* after the digitization module, so that the simulated events can be processed exactly in the same manner as the actual data, producing the same SFFs. This compatibility is very useful for developing the background estimator with *simHXD*.

At the first stage of the digitization module, LYs of the GSO and BGO crystals are calculated from the energy deposits and their positions. Then, the total LY is converted into the output charge of the PMT, randomized by its energy resolution. In this stage, two experimental tables are used in the calculation: 1) the ratio of LYs of GSO crystals to the well and bottom part of the BGO crystals and 2) the energy resolution table of PMTs as a function of the LYs of GSO crystals. Fig. 4(a) shows a scatter plot of LYs of GSO to BGO crystals for 511 keV monochromatic photons irradiated uniformly to a Well unit. The PMT outputs, which are a sum of these two values, are used to judge the trigger status, by comparing with the assumed lower discriminator level. After the event is triggered, calculations are performed for all the 36 units to determine the HIT_PATTERN, and other quality flags are also processed, such as trigger pattern for PIN, an upper discrimination flag, and multiplicity flags. The final stage is to calculate the slow and fast PI channels (SLOW_PI and FAST_PI, respectively), and simulate the electronic PSD algorithm, as demonstrated in Fig. 4(b). The output charge from both GSO and BGO crystals is fully integrated with the slow shaper, so the SLOW_PI is calculated by simply adding the LYs of GSO and BGO. In contrast, the FAST_PI of a BGO event becomes significantly lower than its SLOW_PI, because

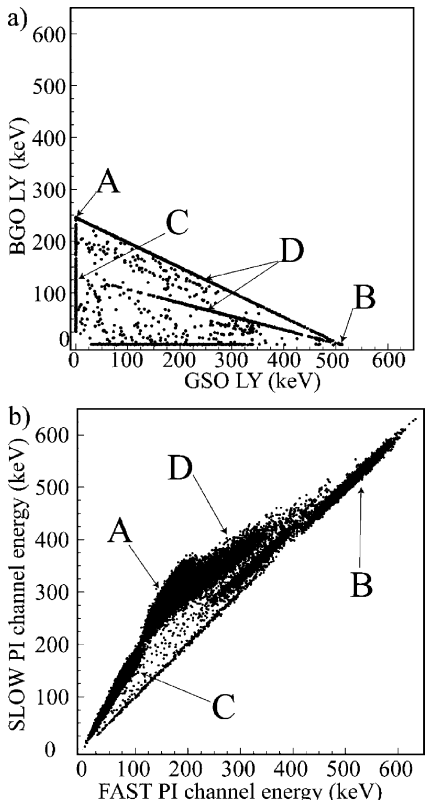

Fig. 4. (a) Scatter plot of the energy deposits of GSO and BGO scintillators calculated by *simHXD* for 511 keV gamma-rays. (b) The slow-fast diagram generated from the same simulation datasets. Marks A, B, and C shows the full deposit events to BGO well part, GSO, BGO bottom part, respectively, and mark D is events Compton-scattered between BGO and GSO crystals.

the slowly decaying BGO crystal is not fully integrated by the fast shaper. Thus, the following effects are included as an experimental table: 1) the charge-integration factor for the BGO crystal with the fast shaper and 2) the ADC spreading for the GSO and BGO crystals of each unit.

There is no plan to release *simHXD* to end users, because its usage would require both the high skill of the Monte Carlo technique and full knowledge of the HXD-II hardware. Instead, all results and products obtained with this simulator are summarized in the public calibration database, and simpler estimation kits will be released after launch. Using these kits, the hit information gathered by the PickupData module (Fig. 2) can be recorded into the simulation database, and its reading module has been prepared to have a compatible interface to connect to the digitization module. This can be switched from the Monte Carlo engine of *simHXD*, and acts as a faster background estimator or a response builder than the full Monte Carlo simulator.

III. Verification of the Simulator

A. Comparison With the Gamma-Ray Irradiation Results

In order to confirm the ground performance of the HXD-II and to fix the calibration parameters listed in Section II-B, an extensive a pre-flight calibration experiment was conducted at ISAS/JAXA Japan using the flight HXD-II sensor and the flight electronics, for two weeks in June 2004. All components

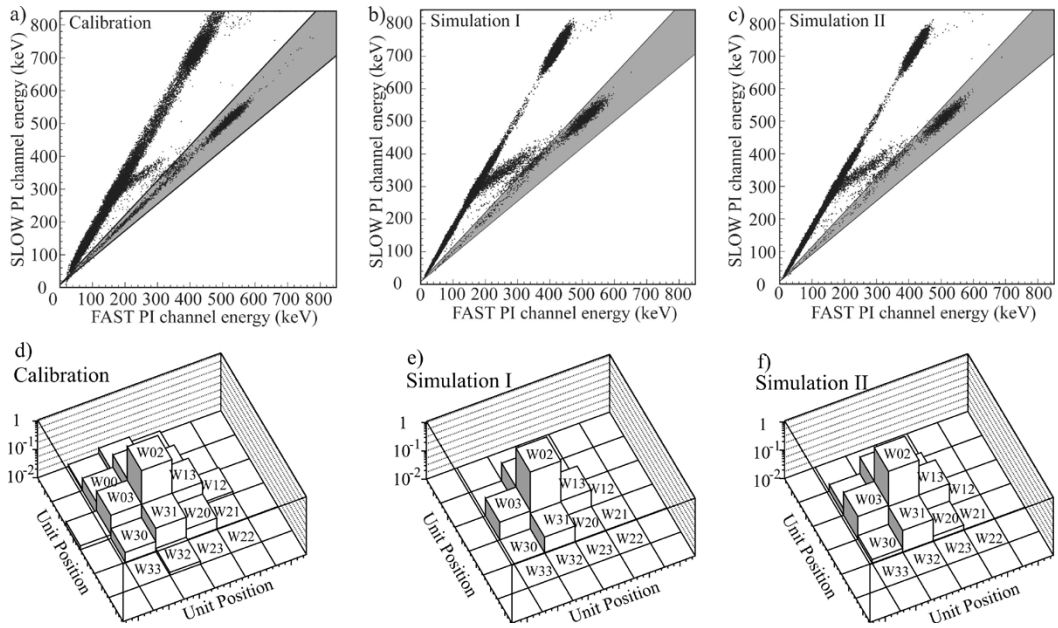

Fig. 5. Comparison of the experimental data for a ^{22}Na irradiation tests (a) and (d) with the simulated data obtained by *simHXD* (others). The top panels [(a), (b), and (c)] show the slow-fast diagrams in PI space. The bottom panels (d), (e), and (f) show the distributions of activated units in HIT_PATTERN, when the trigger is issued by the PMT of a specified Well unit (in this case, W02). The center [(b) and (e)] and right [(c) and (f)] panels were calculated with infinite and finite source distances, respectively (see the text).

of the setup were placed in a low-temperature heat bath kept at -20 °C, which is the operation temperature of the HXD-II sensor in orbit. To control the irradiation position of RIs, the sensor was placed on the side, and an accurately aligned RI attachment board was set on the optical axis of the HXD-II at a distance of 3.1 m from the GSO crystal. The detailed study of the sensor response utilized ^{137}Cs and ^{22}Na, with the nominal event reduction mode coupled with several electronics settings. Relative alignments of the 64 fine collimators were measured by observing ^{133}Ba sources with the PIN diodes. In addition, ^{152}Eu and ^{109}Cd were used for gain measurements.

The slow-fast diagram and the distribution of the HIT_PATTERN obtained by a ^{22}Na (511 keV and 1274 keV photons) irradiation test are shown in Fig. 5(a) and (d). The parameters obtained in this experiment, such as the PMT resolution and LYs (Section II-D) were installed in *simHXD*. Fig. 5(b) and (e) shows the results using these parameters, assuming that all the 511 and 1274 keV primary photons are irradiated in parallel along the optical axis of the HXD-II. This ideal condition is realized only in orbit, and the response matrix for astrophysical use must be calculated with this condition. On ground, the source distance is finite, so a simulation with spherical irradiation from the same distance was also carried out [Fig. 5(c) and (f)].

For a more quantitative comparison, the observed and simulated energy spectra for pure PMT events are shown in Fig. 6(a) in the SLOW_PI space without the GRADE_PSDSEL condition. In the higher energy band, the calculation can reproduce the experimental data within about 5% accuracy, which is acceptable in the pre-flight stage because the value is comparable to the other systematics. Unexplained events in the actual spectra, which are dominant in the lower energy band, are gamma-ray events Compton-scattered by some structures surrounding the experiment setup, including the heat bath and a thick wood table

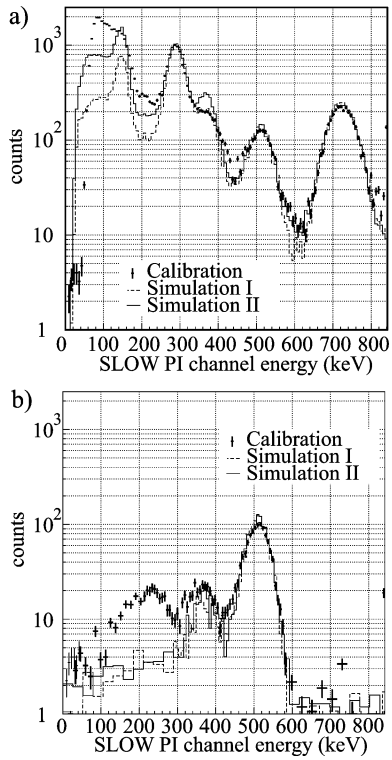

Fig. 6. Same comparison as in Fig. 5, but in the slow PI channel space, for pure PMT events (a) with and (b) without the GRADE_PSDSEL criterion. The selection region is indicated with shadows in Fig. 5 top. The prominent 720 keV peak in the top panel is the 1274 keV photons detected by the BGO bottom piece, of which the LY is about 50% of that of the GSO.

under the HXD-II sensor, because the spectral shape of this component changes as the condition changes.

The two spectra in Fig. 6(b) were obtained by processing the actual and simulated spectra in the identical way using the *crit-*

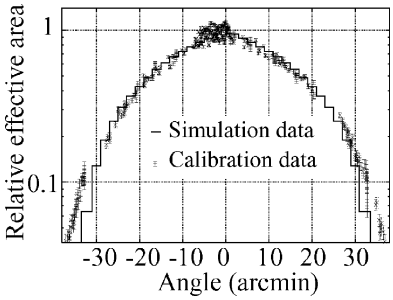

Fig. 7. Comparison of the angular response between the simulation and the experimental data. The crosses show the counts of the photo-absorption peak detected with 64 PIN diodes by ^{133}Ba irradiation experiments, as a function of the angle from the optical axis of the HXD-II along the horizontal and vertical axes of Fig. 1 (right). The data of a PIN appears twice, corresponding these two directions. The individual miss-alignment of fine collimators has been corrected for each PIN. The line shows the results of a simulation of pure PIN events with 31 keV monochromatic irradiation calculation by *simHXD*.

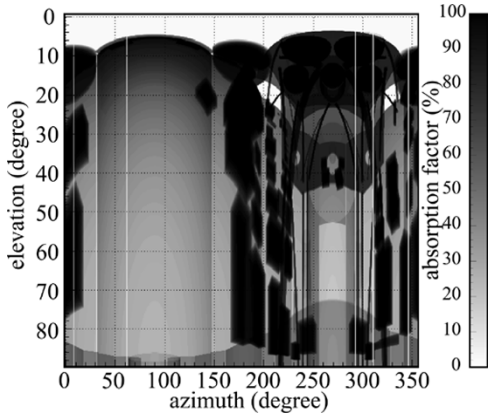

Fig. 8. Absorption map for 511 keV photons obtained by *ShadowAste2*, with the *Astro-E2* satellite geometry on the ground mode; folded optical bench, no solar panel, and without filling Ne refrigerant solid. The horizontal and vertical axis represent the azimuth angle, θ, and negative elevation angle, ϕ, from the optical axis of the HXD-II, respectively. Many structures of the satellite are seen; electric boxes around $\theta = 0°$, 180°–220°, 300°–350°, Ne tank around $\theta = 260°$, $\phi < 50°$, optical bench $\theta = 260°$, $\phi > 40°$, and four X-ray Mirrors $\theta = 220° - 320°$, $\phi \sim 10°$.

ical ftools, (Section II), and retaining only GSO events (with GRADE_PSDSEL). The reproduction is quite acceptable over the main photo-absorption peak, and a weaker structure around the 300–400 keV range. The latter is due to residual Compton branch, formed by those events which are scattered by a GSO crystal and fully absorbed in the BGO bottom part; this structure cannot be reproduced without a digitization module. The low-energy hump in the experimental data around the 240 keV are mixed with events back-scattered by the RI board.

An example of the angular dependence of the effective area, calculated with *simHXD* for 31 keV monochromatic irradiation is shown in Fig. 7. At an energy band lower than 30 keV, where PIN diodes work, the angular response is determined mainly by the photo-absorption process in fine collimators, consisting of 8×8 cells of 160 μm thick phosphor-bronze foils, placed in front of the PIN diode. To verify this distribution, the HXD-II was scanned with a ^{133}Ba source from directions close to the optical axis. As shown in Fig. 7, the simulation result of pure PIN events with PIN GRADEs can describe the experimental data within 2% accuracy in the $\pm$30 arcmin range.

B. Verification of the Satellite Geometry

To achieve an all-sky monitoring observation with the HXD-WAM (Section I), it is important to estimate the absorption coefficient by the satellite components for the 4π direction in the gamma-ray energy band of 50 keV to 5 MeV. For this purpose, *simHXD* with the satellite geometry is needed. The Mass Model of the satellite has been already developed from the *Astro-E* period, and many improvements have been achieved in collaboration with other instrument teams on-board *Astro-E2*, as reported by Ozaki *et al.* [11]. The satellite geometry of *Astro-E2* is already installed into *simHXD*. The results in constructing the HXD-WAM response by several full simulations with *simHXD* to the selected energy and direction of incident photons are reported by Ohno *et al.* [12].

A full Monte Carlo simulation for many parameter sets takes too much time. For the purpose of calculating the absorption probability maps, only the Geant4 geometry with the corresponding material table is needed. To know the absorption coefficient along a direction to research, first step is to list up the geometrical and material parameters for all of the components, i, along the direction, such as atomic number and/or the mixing ratio of the materials, M_i, with the physical length, l_i. The absorption coefficient can be obtained by $\Sigma A(M_i) l_i$, where A is the attenuation coefficient by photoelectric absorption, pair creation, and Compton scattering. Such a code has been developed and tested by the Swift satellite team, called *ShadowSwift* [14]. A similar application to the *ShadowSwift* is publicly available as Sector Shielding Analysis Tool [15]. Thanks to the *Swift* BAT collaborators, the shadow code have been adopted to the *Astro-E2* satellite geometry. The attenuation factor, A, for all the materials and components of *Astro-E2* satellite are prepared using NIST database [16], in addition to our original measurements for some components. This application is called *ShadowAste2*. An example of the absorption map for 511 keV photons obtained by *ShadowAste2* is shown in Fig. 8.

To verify the calculated absorption map, an RI scanning tests around the HXD-WAM were performed at ISAS/JAXA, before and after boarding the satellite in June and September 2004, respectively. The RI were irradiated 3.0 m away from the HXD-II sensor. An example of an azimus angular dependance of counting rates is shown in Fig. 9(a). More experimental results are summarized by Ohno *et al.* [12]. The transmission rate, absorbed by the satellite components, are calculated by dividing two data sets measured before and after boarding the satellite, as shown in Fig. 9(b). The calculation from the absorption map for 1274 keV photons by the *ShadowAste2* is also shown in the figure. In the range of θ from 0° to 170°, where only simple carbon-aluminum-honycomb boards exist, the simulation can reproduce the experimental data within 5% accuracy, but in another range of $\theta = 170° - 350°$, there are large discrepancy between them. One possibility is that the absorption coefficients by several electric boxes are overestimated, and an other possibility is that events Compton scatterd by many structures of the satellite are included in the experimental data, whereas the *ShadowAste2* only consider the

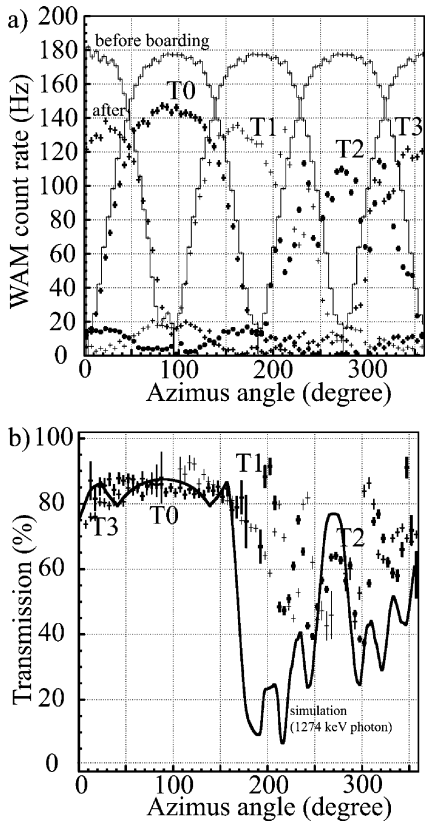

Fig. 9. (a) Results of the RI (100 μCi ^{22}Na) scanning experiment measured with four sides of the WAM counters, named T0, T1, T2, T3, before and after boarding the satellite, for the 1274 keV photons. (b) The comparison of the experimental data (cross) with the simulation with *ShadowAste2*(line).

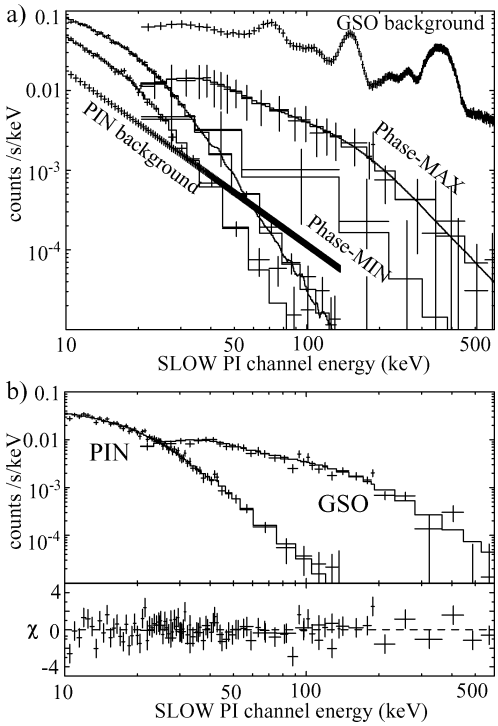

Fig. 10. (a) Expected energy spectra with 80 000 s observation of the astrophysical object PSR B1509-58, for the pulsation phase (phase-MAX) and the dim phase (phase-MIN), with the estimated background spectra [6]. (b) The spectra of the pulsation component.

photoelectric absorption. The discussion using the full Monte Carlo simulator, *simHXD*, are reported by Ohno *et al.* [12].

IV. Pre-Flight Estimation of the HXD Performance

A. Example of the Expected Spectra of Astrophysical Object

The *simHXD* provides many PI spectra for many incident gamma-ray energies, which can be summarized into a response matrix. With the matrix, PIN and GSO PI spectra of known astrophysical objects can be simulated; for example, those of an X-ray emitting star, PSR B1509-58, are shown in Fig. 10(a). The object is one of the well-studied young rotation-powered pulsars exhibiting a periodic pulsation in hard X-ray band with a period of 150.6874 ms [17]. The sensitivity of the HXD-II is determined by the absolute level and the systematic errors of the background. Since the flux at the maximum and minimum pulsation phases comes at one or two order-of-magnitude lower than the background level, respectively, the object must be a good-checking source of the sensitivity. In the figure, an estimation of the in-orbit background by previous work [6] for the period of the minimum solar activity is used. The in-orbit background includes not only the intrinsic background events, which are well measured on many sea-level experiments within a few percent systematics, but also activation events induced by cosmic-ray particles, whose model currently has larger systematics of about 10%, although many verifications via several beam tests of protons and heavy ions with approximately a few hundred MeV/nucleon were archived. On the other hand, in extracting a pulsation component, the background data is the actual (not estimated or not calculated) data measured in the minimum phase, so the statistical error comes dominant compared to the other systematics Therefore, as shown in Fig. 10(b), the spectra of the pulsation component is well determined over a wide energy range of over 400 keV.

B. Stray Light From an Offset Source

Since the HXD-II is a nonimaging detector, photons from an X-ray-bright astrophysical object near an on-axis point can contribute to increase the background level. Thus, larger angular response than that in Fig. 7 is important in orbit. Although the intrinsic angular response of the HXD-II sensor was measured and confirmed with *simHXD* (Section III-A), but the absorption by structures of the *Astro-E2* satellite, must be checked, as considered for the HXD-WAM observation in Section III-B. As shown in Fig. 11, the absorption by the optical bench occurs near the limb of the field of view (FOV) of the HXD-II. A verification experiment is planed to archive several off-set pointing observations of Crab Nebula, after launch.

V. Summary

To derive the incident energy spectra of astrophysical objects from the dataset of the HXD-II on-board *Astro-E2*, the HXD-II software packages of processing tasks and Monte Carlo simulation tools. have been developed. The calibration parameters were listed and measured in pre-flight RI irradiation experiments, and are already installed into the software. Verification

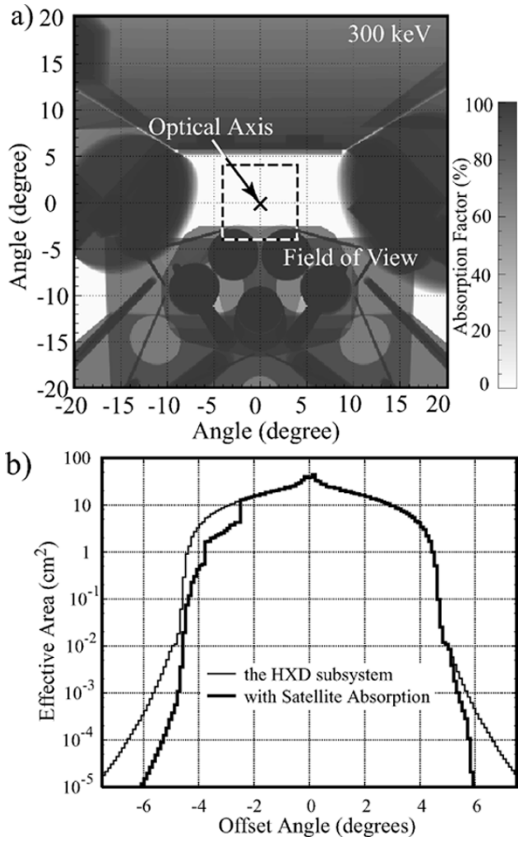

Fig. 11. (a) Absorption map for 300 keV photons by *ShadowAste2*, near the optical axis. (b) The angular response of GSO crystal, calculated with and without the satellite absorption along the vertical axis of the top panel.

checks with comparisons between the experimental and the simulated data have been achieved. Only some parameter tune-up remains. After launch, in addition to the response generator, we have to construct and complete the background estimation toolkit with in-orbit calibration datasets.

REFERENCES

[1] M. Tashiro *et al.*, "Performance of the ASTRO-E hard X-ray detector," *IEEE Trans. Nucl. Sci.*, vol. 49, no. 4, pp. 1893–1897, Aug., 2002.
[2] C. Tanihata *et al.*, "Preflight performance of the Astro-E hard X-ray detector," in *Proc. SPIE*, vol. 3765, 1999, pp. 645–662.
[3] M. Kawaharada *et al.*, "Development and qualification of the HXD-II onboard *Astro-E2*," in *Proc. SPIE*, vol. 5501, 2004, pp. 286–295.
[4] M. Kokubun *et al.*, "Activation of the ASTRO-E hard X-ray detector in low earth orbit," *IEEE Trans. Nucl. Sci.*, vol. 46, no. 3, pp. 371–376, Jun. 1999.
[5] K. Nakazawa *et al.*, "Fabrication of the ASTRO-E hard X-ray detector," in *Proc. SPIE*, vol. 3765, 1999, pp. 148–159.
[6] M. Kokubun *et al.*, "Improvements of the *Astro-E2* hard X-ray detector (HXD-II)," *IEEE Trans. Nucl. Sci.*, vol. 51, no. 5, pp. 1991–1996, Oct. 2004.
[7] Y. Uchiyama *et al.*, "Study of energy response of Gd2SiO5:Ce3+ scintillator for the ASTRO-E hard X-ray detector," *IEEE Trans. Nucl. Sci.*, vol. 48, no. 3, pp. 379–384, Jun. 2001.
[8] M. Sugiho *et al.*, "Spatially dependent response of thick and large area p-i-n diode for ASTRO-E hard X-ray detector," *IEEE Trans. Nucl. Sci.*, vol. 48, no. 3, pp. 426–429, Jun. 2001.
[9] T. Takahashi *et al.*, "The electronic system for the Astro-E hard X-ray detector," in *Proc. SPIE*, vol. 3445, 1998, pp. 155–168.
[10] K. Yamaoka *et al.*, "Development of the HXD anti counters onboard *Astro-E2*," *IEEE Trans. Nucl. Sci.*, to be published.
[11] M. Ozaki *et al.*, "Radiation physics simulator for space X-ray observatory *Astro-E2*," *IEEE Trans. Nucl. Sci.*, to be published.
[12] M. Ohno *et al.*, "Preflight calibration and performance of the *Astro-E2*/HXD-II anti counter as the all sky monitor," *IEEE Trans. Nucl. Sci.*, to be published.
[13] S. Agostinelli *et al.*, "GEANT4—A simulation toolkit," *Nucl. Instrum. Meth. A*, vol. 506, pp. 250–303, 2003.
[14] G. Sato and M. Ajello, Private Communication, Swift BAT Collaborators.
[15] G. Santin *et al.*, "Geant4 for space: Mission simulations and engineering tools," presented at the IEEE Nucl. Sci. Symp., 2003.
[16] M. J. Berger *et al.*. XCOM, Physical Reference Data. NIST. [Online]. Available: http://physics.nist.gov/PhysRefData/Xcom/Text/XCOM.html
[17] S. Gunji *et al.*, *Observation of Pulsed Hard X-Rays/Gamma-Rays from PSR 1509-58*, vol. ApJ 429, pp. 284–291, 1994.